# Structural, Magnetic, and Transport Properties of $Fe_{1\text{-}x}Rh_x$/MgO(001) Films Grown by Molecular-Beam Epitaxy

Antonio B. Mei,[1,*] Yongjian Tang,[2] Jennifer L. Grab,[2] Jürgen Schubert,[3] Daniel C. Ralph,[2,4] and Darrell G. Schlom[1,4]

[1] *Department of Materials Science and Engineering, Cornell University, Ithaca, NY, 14853, USA*
[2] *Physics Department, Cornell University, Ithaca, NY, 14853, USA*
[3] *Peter Grüenberg Institute (PGI-9) and JARA-Fundamentals of Future Information Technology, Forschungszentrum Jüelich GmbH, 52425 Jüelich, Germany*
[4] *Kavli Institute at Cornell for Nanoscale Science, Ithaca, NY, 14853, USA*

$Fe_{1\text{-}x}Rh_x$ layers are grown with varying rhodium fraction $x$ on (001)-oriented MgO substrates by molecular-beam epitaxy. Film structural, morphological, magnetic, and transport properties are investigated. At room temperature, layers are ferromagnetic (FM) for $x < 0.48$ and antiferromagnetic (AF) for $x > 0.48$. Separating the two magnetically ordered phases at $x = 0.48$ is an abrupt change in the $Fe_{1\text{-}x}Rh_x$ lattice parameter of $\Delta a = 0.0028$ nm ($\Delta a/a = -0.9\%$). For AF layers, the FM state is recovered by heating across a first-order phase transition. The transition leads to a large resistivity modulation, $\Delta\rho/\rho = 80\%$, over a narrow temperature range, $\Delta T = 3$ K, in stoichiometric $Fe_{0.50}Rh_{0.50}$/MgO(001). For samples with compositions deviating from $x = 0.50$, fluctuations broaden $\Delta T$ and defect scattering reduces $\Delta\rho/\rho$.

FeRh ($Pm\bar{3}m$, B2, CsCl structure) is a fundamental component in memory cells[1,2], magnetocaloric refrigerators[3,4], and logic devices.[5,6] Its diverse functionality stems from an entropy-driven first-order transition[7] between ferromagnetic (FM) and antiferromagnetic (AF) states which persists when deposited in film form, a prerequisite for integration in device heterostructures. Accompanying the intrinsic magnetic transition is a large resistivity modulation which rivals giant magnetoresistance effects observed in magnetic multilayers.[8,9] Rhodium fraction $x$ is suspected to strongly affect $Fe_{1\text{-}x}Rh_x$ transport characteristics, but its role has not yet been systematically investigated in epitaxial films. Instead, work has focused on understanding size effects,[10,11] annealing treatments,[12–15] and transition mechanics.[16–20] The few compositional studies on $Fe_{1\text{-}x}Rh_x$ films omit transport properties entirely, emphasizing magnetic attributes,[21] or are based on inhomogeneous polycrystalline layers containing secondary phases.[22] Here, we systematically examine the structural, morphological, magnetic, and transport properties as a function of rhodium fraction $x$ of phase-pure epitaxial $Fe_{1\text{-}x}Rh_x$ films with the CsCl structure deposited on (001)-oriented MgO substrates.

$Fe_{1\text{-}x}Rh_x$/MgO(001) films are grown via molecular-beam epitaxy to a thickness of ∼35 nm in a Veeco GEN10 system (base pressure: $1\times10^{-8}$ Torr = 1.3 $\times10^{-6}$ Pa) by simultaneously supplying iron (99.995% pure) and rhodium (99.95% pure) from independent effusion cells. Rhodium fractions $x$ are controlled by adjusting iron and rhodium cell temperatures within 50 °C of 1150 and 1600 °C, respectively, while maintaining a total atomic flux of $\sim4\times10^{13}$ atoms/cm$^2$·s, corresponding to a growth rate of ∼0.3 nm/min. $x$ values determined[24] from Rutherford backscattering spectra agree with x-ray reflectivity (XRR) deposition rate calibrations based on pure iron and rhodium layers (linear correlation coefficient $r$ = 0.997), demonstrating that atomic incorporation probabilities are unaltered by chemistry. From the calibrate atomic fluxes, deposition times are set to produce layers with a thickness of ∼35 nm. A substrate temperature $T_s$ = 420 °C (estimated from a thermocouple in indirect contact with the growth surface and concealed from in-

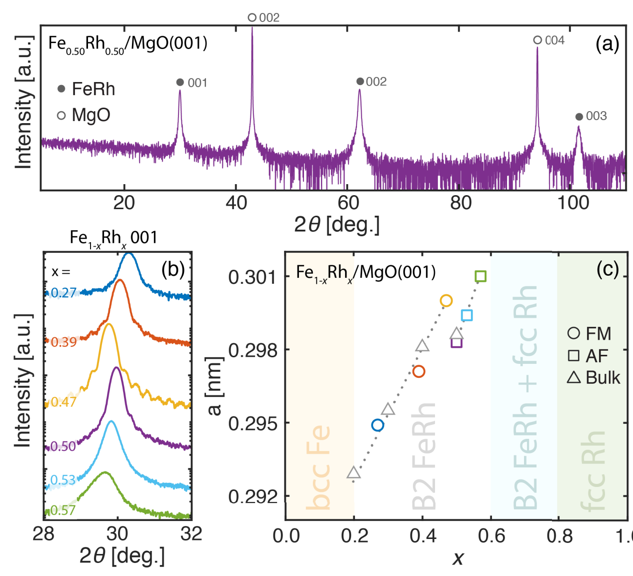


FIG. 1. (a) XRD $\theta$-$2\theta$ scan of a 35-nm-thick stoichiometric $Fe_{0.50}Rh_{0.50}$ film with the B2 CsCl-structure grown on MgO(001) at 420°C by molecular-beam epitaxy. (b) $\theta$-$2\theta$ scans showing the $Fe_{1\text{-}x}Rh_x$ 001 peak for rhodium fractions $0.20 \lesssim x \lesssim 0.60$. (c) Film out-of-plane lattice parameters as a function of composition together with bulk lattice parameters[23] (triangles) for reference. Circles indicate ferromagnetic ordering and squares indicate antiferromagnetic ordering at room temperature.

cident molecular fluxes) is employed for film growth and subsequent 30-min-long *in situ* anneals. High homologous growth temperatures ($T_s/T_\mathrm{m} = 0.37$ for FeRh with melting temperature $T_\mathrm{m} \approx 1600$ °C) are necessary[25] to order bcc $\mathrm{Fe}_{1\text{-}x}\mathrm{Rh}_x$ alloys into the B2 CsCl-structure intermetallic with iron and rhodium residing on distinct positions of the two-atom basis.

X-ray diffraction (XRD) $\theta$-$2\theta$ scans, collected using Cu $K_{\alpha 1}$ radiation (wavelength $\lambda = 0.154056$ nm), establish a phase diagram consisting of four regions: single-phase bcc-Fe(001) ($x \lesssim 0.20$), single-phase B2 $\mathrm{Fe}_{1\text{-}x}\mathrm{Rh}_x$ ($0.20 \lesssim x \lesssim 0.60$), two-phase mixtures of (001)-textured B2 $\mathrm{Fe}_{1\text{-}x}\mathrm{Rh}_x$ and fcc-Rh ($0.60 \lesssim x \lesssim 0.80$), and single-phase fcc-Rh(001) ($x \gtrsim 0.80$). The phase boundaries of our epitaxial films grown on MgO(001) are in close agreement with reports for bulk samples:[23,26] the rhodium-deficient limit, for which the bcc solid solution orders into the CsCl structure, agrees exactly, while the rhodium-rich limit extends 0.08 rhodium fractions above the bulk boundary ($x = 0.52$) due to epitaxial stabilization.[27–31]

A representative XRD $\theta$-$2\theta$ scan is presented in Fig. 1(a) for stoichiometric $\mathrm{Fe}_{0.50}\mathrm{Rh}_{0.50}$/MgO(001). Five peaks are observed over the $2\theta$ range 10-110°: the three reflections at $2\theta = 29.94$, 62.18, and 101.6° are indexed as $\mathrm{Fe}_{0.50}\mathrm{Rh}_{0.50}$ $00l$; the two at 42.92 and 94.05° are identified as MgO $00\underline{2l}$. Sharp mixed-integer film reflections (no systematic absences) indicate CsCl-type ordering. The lack of additional reflections together with pole figure and grazing-incidence scans (not shown) establish that films with $0.20 \lesssim x \lesssim 0.60$ are phase-pure untwinned epitaxial layers oriented with a 45° in-plane rotation with respect to their MgO substrates: $(001)_{\mathrm{Fe}_{1\text{-}x}\mathrm{Rh}_x} \,||\, (001)_\mathrm{MgO}$ and $[110]_{\mathrm{Fe}_{1\text{-}x}\mathrm{Rh}_x} \,||\, [100]_\mathrm{MgO}$.

Diffracted intensities near the $\mathrm{Fe}_{1\text{-}x}\mathrm{Rh}_x$ 001 reflection are plotted as a function of $x$ in Fig. 1(b). As $x$ increases across the single-phase field, $\mathrm{Fe}_{1\text{-}x}\mathrm{Rh}_x$ peaks shift — with one exception — to lower $2\theta$ angles. Figure 1(c) shows out-of-plane lattice parameter $a$ values obtained[32] from $\theta$-$2\theta$ peak positions. $a$ increases approximately linearly from 0.2950 ($x = 0.27$) to 0.3000 nm ($x = 0.47$), contracts sharply to 0.2983 nm ($x = 0.50$), and then continues increasing to 0.3010 ($x = 0.57$). Film lattice parameters values $a(x)$ are in excellent agreement with reports for bulk polycrystals (also shown in Fig. 1(b)).[23] Regression analyses yield a slope of $0.04 \pm 0.01$ nm per rhodium fraction, in close agreement with 0.06 expected based on the larger metallic radius[33] of rhodium (134 pm) versus iron (126 pm), suggesting that rhodium substitutes for iron across the $\mathrm{Fe}_{1\text{-}x}\mathrm{Rh}_x$ single-phase field. The lattice parameter discontinuity of $\Delta a = 0.0028$ nm ($\Delta a/a = -0.9\%$) at $x = 0.48$ occurs as $\mathrm{Fe}_{1\text{-}x}\mathrm{Rh}_x$ undergoes a first-order transition[7] from a FM ($x < 0.48$) to an AF ($x > 0.48$) state.[34] The contracted AF cell corresponds to the new equilibrium geometry[35] after spins ferromagnetically aligned on iron (3.2 $\mu_B$) and rhodium (0.9 $\mu_B$) leave rhodium (0.0 $\mu_B$) magnetically inactive and reorganize antiferromagnetically along {001} on iron (3.3 $\mu_B$).[26,36,37]

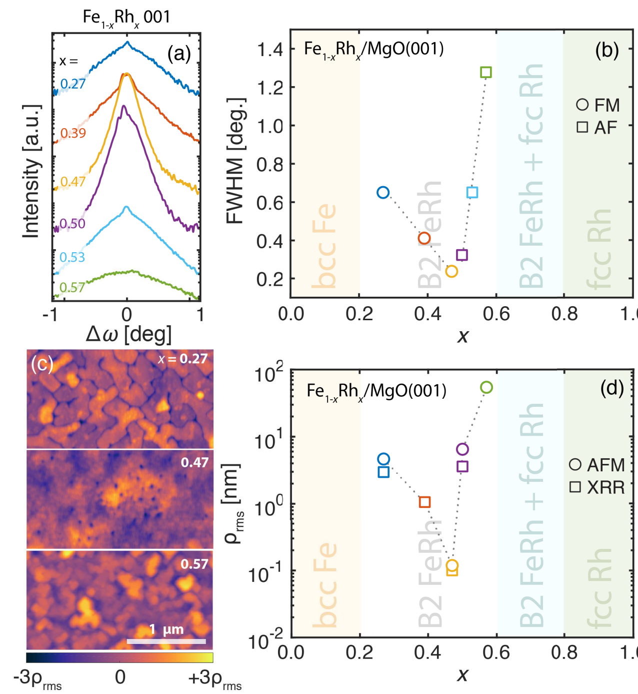


FIG. 2. (a) XRD $\omega$-rocking curve scans of $\mathrm{Fe}_{1\text{-}x}\mathrm{Rh}_x$ 001 reflections and (b) corresponding FWHM values as a function of rhodium fraction $x$. (c) Representative AFM height images of $\mathrm{Fe}_{1\text{-}x}\mathrm{Rh}_x$/MgO(001) layers as a function of composition $x$ across the B2 single-phase field. MgO[100] and $\mathrm{Fe}_{1\text{-}x}\mathrm{Rh}_x$[110] are aligned with the horizontal image axis. (d) Root-mean-square surface roughness values determined as a function of $x$ independently from XRR and AFM.

The structural quality of the films is assessed from $\omega$-rocking curves of $\mathrm{Fe}_{1\text{-}x}\mathrm{Rh}_x$ 001 reflections and atomic force microscopy (AFM) elevation maps. Rocking curve scans and corresponding peak full-width-at-half-maxima (FWHM) are plotted in Figs. 2(a) and 2(b). Reflections are broad at $x = 0.27$ and 0.57 due to mosaicity, but sharpen as $x$ approaches 0.50. FWHM values decrease from 0.65° ($x = 0.27$) and 1.28° ($x = 0.57$) to 0.23° ($x = 0.47$) and 0.32° ($x = 0.50$) indicating increasing crystalline perfection. MgO 002 rocking curves, measured for reference, are found to consist of split peaks with individual peak FWHM values of ∼0.005° (18 arcsec) and an ensemble FWHM of ∼0.06° (216 arcsec); the splitting results from the formation of domains spanning a few millimeters in length and are a common problem commercial substrates.[38]

Figure 2(c) are representative AFM height images. Root-mean-square surface roughness values determined independently from AFM and XRR (not shown) are plotted as a function of $x$ in Fig. 2(d). At $x = 0.27$, the surface morphology ($\rho_\mathrm{rms} = 3.0$ nm) is comprised of 150-nm-wide mesas separated by 1.5-nm-deep trenches preferentially aligned along $\mathrm{Fe}_{1\text{-}x}\mathrm{Rh}_x$ ⟨100⟩. Such features are the hallmark of unfavorable substrate wetting and three-dimensional island growth.[39] For $x = 0.47$, the mesas fuse

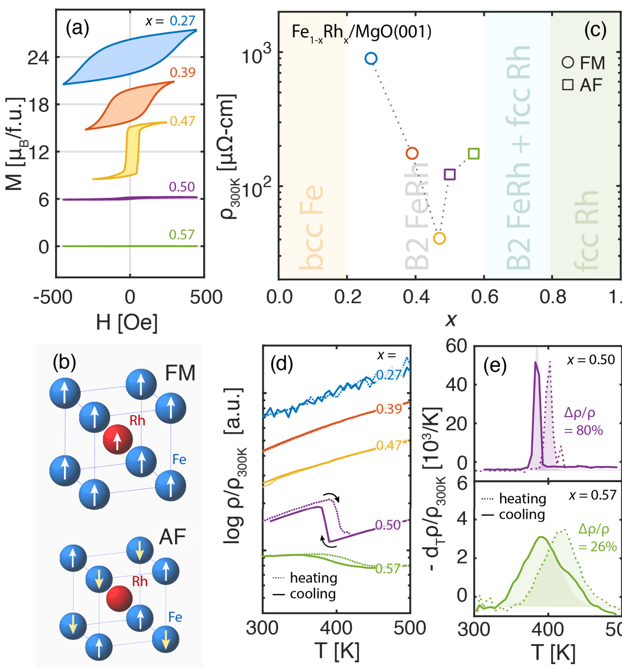


FIG. 3. (a) Magnetization $M$ of $Fe_{1\text{-}x}Rh_x$/MgO(001) films versus applied magnetic field $H$ as a function of rhodium fraction $x$. Curves are offset by 6 $\mu_B$/f.u. for clarity. (b) The crystal structure and spin configurations of ferromagnetic (FM: $x < 0.48$) and antiferromagnetic (AF: $x > 0.48$) $Fe_{1\text{-}x}Rh_x$. (c) Room-temperature $Fe_{1\text{-}x}Rh_x$ resistivities $\rho_{300K}(x)$ for $x$ = 0.20 through 0.80, spanning the B2 single-phase field. (d) Temperature-dependent resistivities $\rho(T)$ as a function of $x$; curves are vertically offset for clarity. (e) Negative temperature-derivative of $\rho(T)$ for samples exhibiting AF-FM transitions ($0.48 < x \lesssim 0.60$).

leaving a smooth surface with sub-monolayer height fluctuations ($\rho_{\rm rms} = 0.1$ nm). Further increasing $x$ to 0.57 is accompanied by the appearance of mounds faceted along $Fe_{1\text{-}x}Rh_x$ $\langle 100 \rangle$ due to the combination of high surface energies and high diffusivities.[40,41] Thus, the smoothest films with the highest structural perfection are obtained near $x = 0.50$.

Figure 3(a) shows the in-plane room-temperature magnetization $M$ of $Fe_{1\text{-}x}Rh_x$/MgO(001) films measured as a function of applied magnetic field $H$ using a vibrating sample magnetometer. Films with $x \leq 0.48$ display hysteretic behavior characteristic of FM ordering with saturation magnetizations of $\sim 4\mu_B$/f.u., consistent with prior reports.[36] Coercive fields $H_c$, defined as the value of $H$ where $M$ changes maximally, decrease with increasing $x$ from 235 ($x = 0.27$) to 129 ($x = 0.39$) and 59 Oe ($x = 0.47$). Fitting $H_c(x)$ with a mean-field behavior, $H_c \propto \sqrt{x - x_c}$, yields a critical rhodium fraction of $x_c = 0.48$ below which $Fe_{1\text{-}x}Rh_x$ is FM. For $x$ above $x_c$, $Fe_{1\text{-}x}Rh_x$ films are macroscopically demagnetized at room temperature, but recover their magnetization when heated above ∼400 K. Since symmetries are necessarily restored by heating across any phase transition,[42] the loss of magnetization in films with $x > 0.48$ implies AF ordering, for which heating leads to the recovery of additional symmetry operations and the emergence of a FM state. These conclusions are in agreement with Mössbauer spectroscopy[26] and neutron scattering[36] results. The crystal structure and spin configurations of ferromagnetic and antiferromagnetic $Fe_{1\text{-}x}Rh_x$ is illustrated in Figure 3(b).

Room-temperature resistivities $\rho_{\rm 300K}(x)$ of ∼35-nm-thick $Fe_{1\text{-}x}Rh_x$/MgO(001) films are shown in Fig. 3(c). As $x$ is varied across the single-phase field, $\rho_{\rm 300K}$ decreases from 898.3 $\mu\Omega$·cm ($x$ = 0.27) to 40.9 $\mu\Omega$·cm ($x$ = 0.47), rises rapidly to 122.3 $\mu\Omega$·cm ($x$ = 0.50), and continues increasing slowly to 174.9 $\mu\Omega$·cm ($x$ = 0.57). The resistivity obtained here for stoichiometric $Fe_{0.50}Rh_{0.50}$, which represents the lowest value reported in the literature,[43] reflects the structural perfection and chemical purity of the layer. The large $\rho_{\rm 300K}(x)$ values near the $Fe_{1\text{-}x}Rh_x$ phase field boundaries stem predominately from increased structural disorder.

Temperature-dependent $Fe_{1\text{-}x}Rh_x$ resistivities $\rho(T)$ between 300 and 500 K are plotted in Fig. 3(d). For rhodium-deficient films ($0.27 \leq x \leq 0.47$), $\rho(T)$ increase linearly with $T$ demonstrating metallic phonon-limited conduction. The superposition of resistivity curves measured during heating and cooling reflect the stability of these layers in air. At $x$ = 0.50, a drop in resistivity is observed near $T_c \approx 392$ K, associated with a transition[7] between AF ($T < T_c$) and FM ($T > T_c$) states. The negative derivative of $\rho(T)/\rho_{300K}$, plotted in Fig. 3(d), shows that the transition is sharp, hysteretic, and symmetric — attributes consistent with first-order transitions — and occurs at 385±3 and 401±3 K during heating and cooling, respectively. The pronounced modulation in resistivity observed, $\Delta\rho/\rho \equiv (\rho_{\rm AF} - \rho_{\rm FM})/\rho_{\rm FM}$ = 80%, represents the highest thermally-induced value reported[6,10,22,43–45] and is consistent with the 85±6% theoretical maximum realizable for well ordered films;[22] the narrow transition widths, $\Delta T = 3$ K, are the smallest observed to date.[6,10,11,22,43–45] For bulk stoichiometric samples, a comparable resistivity change was observed at room temperature by driving the AF-FM transition with pulsed magnetic fields exceeding 15 T; thermally-induced resistivity changes were not investigated, but a $T_c$ of 405 K, in close agreement with our measured values, was deduced from temperature-dependent heat capacity measurements.[46]

Rhodium-rich films with $x = 0.57$ also exhibit a similar transition. In this case, the resistivity changes by only 26% (versus 80% for $x = 0.50$) as AF regions slowly transform into FM domains at 418±32 K and back at 393±40 K (Figs. 3(c) and 3(d)). The smaller $\Delta\rho/\rho$ values for $x$ = 0.57 results from defect scattering, which simultaneously raises $\rho_{\rm AF}$ and $\rho_{\rm FM}$. The broader transition stems from fluctuations, as expected for a film characterized by chemical disorder, crystalline mosaicity, and high surface roughness.

In summary, ∼35-nm-thick epitaxial $Fe_{1\text{-}x}Rh_x$

/MgO(001) films are grown at 420 °C by molecular-beam epitaxy and systematically investigated as a function of rhodium fraction $x$. Within the CsCl-structure $Fe_{1\text{-}x}Rh_x$ single-phase field ($0.20 \lesssim x \lesssim 0.60$), rhodium replaces iron producing a linearly increasing lattice parameter due to its larger metallic radius (134 versus 126 pm)[33]. B2 CsCl-type ordering is established by pronounced x-ray diffraction from mixed-integer film reflections. A lattice parameter discontinuity of $\Delta a = 0.0028$ nm ($\Delta a/a = -0.9\%$) is observed at $x_c = 0.48$, below (above) which films are FM (AF). The perfection and surface smoothness of the layers are optimized near $x = 0.50$. Room-temperature resistivities $\rho_{300K}(x)$ exhibit a minimum of 40.9 $\mu\Omega$·cm at $x = 0.47$. For AF layers ($x \geq 0.48$), FM ordering can be recovered by heating across the first-order phase transition. Temperature-dependent resistivity measurements demonstrate sharp, hysteretic, and symmetric transitions at 385±3 K and 401±3 K during heating and cooling of stoichiometric $Fe_{0.50}Rh_{0.50}$/MgO(001) films. The large resistivity modulation achieved, $\Delta\rho/\rho = 80\%$, represents the largest thermally-induced value observed to date for $Fe_{1\text{-}x}Rh_x$ films. In rhodium-rich layers, the transition is broadened by fluctuations and the percent resistivity change is reduced due to defect scattering.

## I. ACKNOWLEDGEMENTS

The authors thank K. Palmen and W. Zander for their help performing RBS measurements. A.B.M., Y.T., J.L.G., and D.G.S. acknowledge support in part by the Semiconductor Research Corporation (SRC) under nCORE tasks 2758.001 and 2758.003, and by the NSF under the E2CDA program (ECCS-1740136). Materials synthesis was performed in a facility supported by the National Science Foundation (Platform for the Accelerated Realization, Analysis, and Discovery of Interface Materials (PARADIM)) under Cooperative Agreement No. DMR-1539918. This work made use of the Cornell Center for Materials Research (CCMR) Shared Facilities, which are supported through the NSF MRSEC program (No. DMR-1719875). Substrate preparation was performed in part at the Cornell NanoScale Facility, a member of the National Nanotechnology Coordinated Infrastructure (NNCI), which is supported by the NSF (Grant No. ECCS-1542081).

* amei2@illinois.edu

[1] J.-U. Thiele, S. Maat, and E. E. Fullerton, Appl. Phys. Lett. **82**, 2859 (2003).
[2] X. Marti, I. Fina, C. Frontera, J. Liu, P. Wadley, Q. He, R. J. Paull, J. D. Clarkson, J. Kudrnovský, I. Turek, J. Kuneš, D. Yi, J.-H. Chu, C. T. Nelson, L. You, E. Arenholz, S. Salahuddin, J. Fontcuberta, T. Jungwirth, and R. Ramesh, Nat. Mater. **13**, 367 (2014).
[3] Y. Liu, L. C. Phillips, R. Mattana, M. Bibes, A. Barthélémy, and B. Dkhil, Nat. Commun. **7**, 11614 (2016).
[4] K. Nishimura, Y. Nakazawa, L. Li, and K. Mori, Materials Transactions **49**, 1753 (2008).
[5] J. T. Heron, J. L. Bosse, Q. He, Y. Gao, M. Trassin, L. Ye, J. D. Clarkson, C. Wang, J. Liu, S. Salahuddin, D. C. Ralph, D. G. Schlom, J. Íñiguez, B. D. Huey, and R. Ramesh, Nature **516**, 370 (2014).
[6] Y. Lee, Z. Q. Liu, J. T. Heron, J. D. Clarkson, J. Hong, C. Ko, M. D. Biegalski, U. Aschauer, S. L. Hsu, M. E. Nowakowski, J. Wu, H. M. Christen, S. Salahuddin, J. B. Bokor, N. A. Spaldin, D. G. Schlom, and R. Ramesh, Nat. Commun. **6**, 189 (2015).
[7] M. Fallot, Ann. Phys. **11**, 291 (1938).
[8] M. Baibich, J. Broto, A. Fert, N. V. D. F, F. Petroff, P. Etienne, G. Creuzet, A. Friederich, and J. Chazelas, Phys. Rev. Lett. **61**, 2472 (1988).
[9] G. Binasch, P. Grünberg, F. Saurenbach, and W. Zinn, Phys. Rev. B **39**, 4828 (1989).
[10] V. Uhlíř, J. A. Arregi, and E. E. Fullerton, Nat. Commun. **7**, 13113 (2016).
[11] A. Ceballos, Z. Chen, O. Schneider, C. Bordel, L.-W. Wang, and F. Hellman, Appl. Phys. Lett. **111**, 172401 (2017).
[12] J. Cao, N. T. Nam, S. Inoue, H. Y. Y. Ko, N. N. Phuoc, and T. Suzuki, J. Appl. Phys. **103**, 07F501 (2008).
[13] M. A. de Vries, M. Loving, A. P. Mihai, L. H. Lewis, D. Heiman, and C. H. Marrows, New J. Phys. **15**, 013008 (2013).
[14] J. P. Ayoub, C. Gatel, C. Roucau, and M. J. Casanove, Journal of Crystal Growth **314**, 336 (2011).
[15] K. Aikoh, S. Kosugi, T. Matsui, and A. Iwase, J. Appl. Phys. **109**, 07E311 (2011).
[16] C. Bordel, J. Juraszek, D. W. Cooke, C. Baldasseroni, S. Mankovsky, J. Minár, H. Ebert, S. Moyerman, E. E. Fullerton, and F. Hellman, Phys. Rev. Lett. **109**, 117201 (2012).
[17] S. Mankovsky, S. Polesya, K. Chadova, H. Ebert, J. B. Staunton, T. Gruenbaum, M. A. W. Schoen, C. H. Back, X. Z. Chen, and C. Song, Phys. Rev. B **95**, 155139 (2017).
[18] A. Heidarian, S. Stienen, A. Semisalova, Y. Yuan, E. Josten, R. Hübner, S. Salamon, H. Wende, R. A. Gallardo, J. Grenzer, K. Potzger, R. Bali, S. Facsko, and J. Lindner, Phys. Status Solidi B **254**, 1700145 (2017).
[19] P. M. Derlet, Phys. Rev. B **85**, 174431 (2012).
[20] J. B. Staunton, R. Banerjee, M. d. S. Dias, A. Deak, and L. Szunyogh, Phys. Rev. B **89**, 54427 (2014).
[21] S. Inoue, H. Y. Y. Ko, and T. Suzuki, IEEE Trans. Magn. **44**, 2875 (2008).
[22] J. van Driel, R. Coehoorn, G. J. Strijkers, E. Brück, and F. R. de Boer, J. Appl. Phys. **85**, 1026 (1999).
[23] G. Shirane, C. W. Chen, P. A. Flinn, and R. Nathans, Phys. Rev. **131**, 183 (1963).
[24] I. Petrov, M. Braun, T. Fried, and H. E. Sätherblom, J. Appl. Phys. **54**, 1358 (1983).
[25] C. P. Flynn, J. Phys. F **18**, L195 (2000).

[26] G. Shirane, C. W. Chen, P. A. Flinn, and R. Nathans, J. Appl. Phys. **34**, 1044 (1963).

[27] A. Zunger and D. M. Wood, Journal of Crystal Growth **98**, 1 (1989).

[28] R. Bruinsma and A. Zangwill, Journal de Physique **47**, 2055 (1986).

[29] A. R. Kaul, O. Y. Gorbenko, and A. A. Kamenev, Russ. Chem. Rev. **73**, 932 (2004).

[30] E. S. Machlin and T. J. Rowland, *Synthesis and Properties of Metastable Phases*, Proceedings of a Symposium (The Metallurgical Society of AIME, Warrendale, 1980).

[31] C. P. Flynn, Phys. Rev. Lett. **57**, 599 (1986).

[32] J. B. Nelson and D. P. Riley, Proceedings of the Physical Society **57**, 160 (1945).

[33] N. N. Greenwood and A. Earnshaw, *Chemistry of the Elements* (Elsevier, 2012).

[34] M. Ibarra and P. Algarabel, Phys. Rev. B **50**, 4196 (1994).

[35] M. E. Gruner, E. Hoffmann, and P. Entel, Phys. Rev. B **67**, 64415 (2003).

[36] G. Shirane, R. Nathans, and C. W. Chen, Phys. Rev. **134**, A1547 (1964).

[37] S. Maat, J. U. Thiele, and E. E. Fullerton, Phys. Rev. B **72**, 214432 (2005).

[38] J. L. Schroeder, A. S. Ingason, J. Rosen, and J. Birch, Journal of Crystal Growth **420**, 22 (2015).

[39] C. W. Barton, T. A. Ostler, D. Huskisson, C. J. Kinane, S. J. Haigh, G. Hrkac, and T. Thomson, Nature Publishing Group **7**, 44397 (2017).

[40] I. Petrov, P. B. Barna, L. Hultman, and J. E. Greene, J. Vac. Sci. Technol. A **21**, S117 (2003).

[41] J. A. Thornton, J Vac Sci Technol **12**, 830 (1975).

[42] P. M. Chaikin and T. C. Lubensky, *Principles of Condensed Matter Physics* (Cambridge University Press, 2000).

[43] Z. Q. Liu, L. Li, Z. Gai, J. D. Clarkson, S. L. Hsu, A. T. Wong, L. S. Fan, M.-W. Lin, C. M. Rouleau, T. Z. Ward, H. N. Lee, A. S. Sefat, H. M. Christen, and R. Ramesh, Phys. Rev. Lett. **116**, 097203 (2016).

[44] J. D. Clarkson, I. Fina, Z. Q. Liu, Y. Lee, J. Kim, C. Frontera, K. Cordero, S. Wisotzki, F. Sánchez, J. Sort, S. L. Hsu, C. Ko, L. Aballe, M. Foerster, J. Wu, H. M. Christen, J. T. Heron, D. G. Schlom, S. Salahuddin, N. Kioussis, J. Fontcuberta, X. Marti, and R. Ramesh, Nature Publishing Group **7**, 15460 (2017).

[45] C. Le Graët, M. A. de Vries, M. McLaren, R. M. D. Brydson, M. Loving, D. Heiman, L. H. Lewis, and C. H. Marrows, J Vis Exp , 50603 (2013).

[46] P. A. Algarabel, M. R. Ibarra, C. Marquina, A. del Moral, J. Galibert, M. Iqbal, and S. Askenazy, Appl. Phys. Lett. **66**, 3061 (1995).